Statistics of tens-of-photons states scattered by optical cavities, two-level atoms, and Jaynes-Cummings emitters

Jia-Nan Wu,[1] Bingsuo Zou,[2] and Yongyou Zhang [1,*]

[1]*Beijing Key Laboratory of Nanophotonics and Ultrafine Optoelectronic Systems, School of Physics,*
Beijing Institute of Technology, Beijing 100081, China
[2]*MOE and Guangxi Key Laboratory of Processing for Non-ferrous Metals and Featured Materials,*
School of Physical Science and Technology, Guangxi University, Nanning 530004, China

Quantum technology is highly relevant to manipulating photon states, for which the quantum waveguide serves as a primary building block. It is a vital task to explore the statistics of tens-of-photons states in quantum waveguides coupled to quantum emitters, such as optical cavities (OCs), two-level atoms (TLAs), and Jaynes-Cummings emitters (JCEs). However, the related theoretical framework has not been established. Here, we use matrix-product-state theory and show that although OCs do not change the second-order photon-photon correlation $g^{(2)}$, they can tune the occupation ratio of bunching photons η. What is more, the states scattered by TLAs and JCEs exhibit extremely different statistical behaviors in tens-of-photons cases with respect to those in few-photon ones. The scattering effects from JCEs tend to those from OCs as photon number $n \to \infty$, and photon-photon correlation due to JCEs reaches a maximum value as n increases. We anticipate these distinguishable results for tens-of-photons states will be a starting point for multiphoton manipulation in quantum waveguides.

I. INTRODUCTION

The dynamics of quantum many-body systems [1–6] present intriguing challenges that consistently captivate researchers' attention. Notably, the intricate dynamics of multiphoton phenomena have been extensively explored [7–13] since photons are optimal carriers for quantum information. Manipulating photons is a pivotal technology for optical quantum computers [14]. The realm of waveguide-QED systems [15–19], which encompasses one-dimensional (1D) waveguides and quantum emitters like optical cavities (OCs) [20–22], two-level atoms (TLAs) [23], and Jaynes-Cummings emitter (JCEs) [15], provides a straightforward yet effective platform for the study of the multiphoton manipulation.

Building upon these systems, researchers have contributed a lot of theoretical [7–13,21,23–25] and experimental [26–28] studies pertaining to multiphoton transport [16,21,23,24,26], correlations [12,24,28,29], bunching and antibunching behaviors [29], entanglements [25,27,30], bound states [31], and more. In these reported works, researchers proposed the Bethe-ansatz approach [7], Lehmann-Symanzik-Zimmermann reduction [21,32,33], Green's-function decomposition of multiple-particle-scattering matrices [34], input-output formalism [35–38], Feynman-diagram formalism [21], and so on. According to these methods, the statistics for the few-photon states scattered by quantum emitters like OCs [21], TLAs [11], and JCEs [11,36] have been studied. As for few-photon cases, the TLA results in a bunching behavior

in the transmitted state but in an antibunching behavior in the reflected state [29]. The OCs lead to the photon-blockade effects in the strong-coupling regime [21].

Recalling the philosophy of "more is different" [39] by Anderson, novel phenomena should appear in the scattering process of the states with many more than one photon. Regretfully, the methods listed above suit only the systems involving a few (generally, no more than four) photons. The main challenge they face is the exponential growth of the Hilbert spaces. To overcome it, we turn to matrix-product-state (MPS) theory [40–43], which draws inspiration from the principles of the density-matrix renormalization group [44,45] and offers an intelligible framework for studying 1D quantum many-body states [40,42]. This theory has been adeptly employed in examining the temporal evolution of strong-correlation systems [42,46,47], including 1D spin chains [1,48,49] and the Bose-Hubbard model [50].

In waveguide-QED systems, MPS theory has found application in the scattering behavior of few-photon states [51,52]. This study expands the MPS theory to investigate the statistical properties of tens-of-photons states within waveguide-QED systems, scattered by OCs, TLAs, and JCEs. The efficacy of MPS theory is validated by demonstrating that scattering events involving OCs preserve the straight-product property of the initial Fock states, as evidenced by the second-order correlation function $g^{(2)} \equiv 1 - \frac{1}{n}$ (n is the total photon number). But the scattering of OCs tunes the occupation ratio of bunching photons η. However, the states scattered by TLAs and JCEs exhibit extremely different statistical behaviors in tens-of-photons cases with respect to few-photon ones. As n increases, the photon-photon correlations induced by JCEs
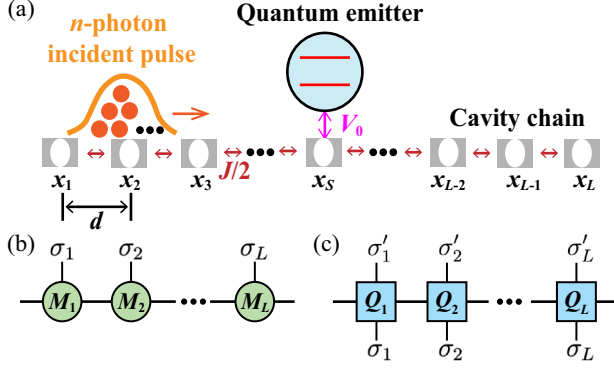
FIG. 1. (a) Schematic of a quantum emitter side coupled to the Sth cavity of a cavity chain whose lth cavity is located at $x_l = (l-1)d$. An incident pulse with n photons is demonstrated. (b) and (c) Tensor networks for the MPS and MPO with physical indices $\{\sigma_l\}$ and $\{\sigma_l, \sigma_l'\}$, respectively.

reach a maximum value when the pulse has several photons from the perspective of transmission, and JCE-induced scattering tends to resemble the OC-induced scattering as $n \to \infty$. What is more, η monotonously grows as n increases for all three types of quantum emitters but remains less than that in the initial states.

This work is organized as follows. In Sec. II, the framework of the MPS method is introduced for the scattered states. Section III discusses the photon-number distributions, transmissions, second-order correlation functions, and occupation ratios of bunching photons for tens-of-photons states. Finally, the conclusions and outlook are summarized in Sec. IV.

II. METHOD

We use the waveguide-QED system drawn in Fig. 1(a) as the cornerstone to present the way to establish the MPS framework. To meet the requirements of the MPS framework, the waveguide is approximated as a cavity chain, with site number L, lattice constant d, and nearest-neighbor hopping $J/2$. All the cavities hold identical eigenfrequencies ω_W. The Sth cavity is coupled to the quantum emitter, and the incident n-photon pulse is denoted by the orange curve and solid dots. The chain dispersion is $\varepsilon = \omega_W - J\cos(kd)$ [53,54]. Such a lattice is described by the Hamiltonian,

$$\hat{H} = \hat{H}_W + \hat{H}_E + \hat{H}_I, \tag{1}$$

where $\hat{H}_W$, $\hat{H}_E$, and $\hat{H}_I$ respectively correspond to the cavity chain, quantum emitter, and interaction between them. They read

$$\hat{H}_W = \sum_{l=1}^{L} \omega_W \hat{a}_l^\dagger \hat{a}_l - \frac{J}{2}\sum_{l=1}^{L-1}(\hat{a}_l^\dagger \hat{a}_{l+1} + \text{H.c.}), \tag{2}$$

$$\hat{H}_E = \omega_c \hat{a}_c^\dagger \hat{a}_c + \omega_a \hat{\sigma}^+ \hat{\sigma}^- + \Omega(\hat{a}_c^\dagger \sigma^- + \sigma^+ \hat{a}_c), \tag{3}$$

$$\hat{H}_I = V_0(\hat{a}_S^\dagger \hat{a}_c + \text{H.c.}). \tag{4}$$

Here, the Planck constant is set to $\hbar = 1$ for convenience. $\hat{a}_l^\dagger$ ($\hat{a}_l$) represents the creation (annihilation) operator of the lth cavity in the chain. $\hat{H}_E$ takes the JCE as an example, where $\hat{a}_c^\dagger$ ($\hat{a}_c$) is the creation (annihilation) operator of the cavity

in the JCE and σ^+ (σ^-) is the raising (lowering) operator of the corresponding TLA. Ω describes the Rabi coupling between them. If the quantum emitter is an OC or TLA, $\hat{H}_E$ can be simplified, i.e., taking $\omega_a = \Omega = 0$ for the OC case or taking $\omega_c = \Omega = 0$ for the TLA case. V_0 measures the coupling between the quantum emitter and the Sth cavity in the chain. If the emitter is a TLA, $\hat{a}_c$ in Eq. (4) should be changed to $\hat{\sigma}^-$.

To apply the MPS method, we write the multiphoton states in the following MPS form, whose tensor network is presented in Fig. 1(b):

$$|\Phi\rangle_n = \sum_{\{\sigma\}} M_1^{[n]\sigma_1} M_2^{[n]\sigma_2} \cdots M_L^{[n]\sigma_L} |\sigma_1 \sigma_2 \cdots \sigma_L\rangle, \tag{5}$$

where σ_l is the occupation number on the lth site and n is the total one with $\sigma_l \leqslant n$. $\{\sigma\}$ represents the set of $\{\sigma_1, \sigma_2, \ldots, \sigma_L\}$. The matrix of $M_l^{[n]\sigma_l}$ rests on the lth site [see Fig. 1(b)], where $[n]$ means that there are n excitations in $|\Phi\rangle_n$. $M_1^{[n]\sigma_1}$ is a one-row matrix, while $M_L^{[n]\sigma_L}$ is a one-column one. We take the n-photon Gaussian pulse

$$|i\rangle_n = \sum_{l_1, l_2, \ldots, l_n} \phi_{l_1} \phi_{l_2} \cdots \phi_{l_n} \hat{a}_{l_1}^\dagger \hat{a}_{l_2}^\dagger \cdots \hat{a}_{l_n}^\dagger |\varnothing\rangle \tag{6}$$

as an example, where $|\varnothing\rangle$ is the vacuum state. The coefficient ϕ_l reads $\phi_l = N \sum_k e^{-(k-k_0)^2/k_w^2} e^{-ik(x_l - x_0)}$, with N being the normalized constant and the wave vector $k = \frac{2\pi}{L} l$ ($l = 1, 2, \ldots, L$). This ϕ_l, with the central wave vector k_0, the central energy $\varepsilon_0 = \omega_W - J\cos k_0 d$, the central position x_0, and the width $2k_w^{-1}$, guarantees the invariance of $|i\rangle_n$ under the exchange of any two photons. Note that $|i\rangle_n$ is a product Fock state.

The first step for the MPS theory is to transform $|i\rangle_n$ into the form of Eq. (5). This is not a trivial task, especially for the cases with large n and L, because of the exponential increase of the Hilbert space. The relation $|i\rangle_n = (\sum_{l_n} \phi_{l_n} \hat{a}_{l_n}^\dagger)|i\rangle_{n-1}$ suggests that we establish an iterative relation between the MPS forms of $|i\rangle_n$ and $|i\rangle_{n-1}$. The procedure (see Sec. A 1) includes (1) writing the single-occupation state $\phi_{l_1} \hat{a}_{l_1}^\dagger |\varnothing\rangle$ in the MPS form, (2) constructing the MPS form of $|i\rangle_1$ by superposing the MPSs of all $\phi_{l_1} \hat{a}_{l_1}^\dagger |\varnothing\rangle$, (3) deriving the iteration relation between the MPSs of $\phi_{l_n} \hat{a}_{l_n}^\dagger |i\rangle_{n-1}$ and $|i\rangle_{n-1}$, and (4) similar to step 2, constructing the MPS form of $|i\rangle_n$ by superposing the MPSs of all $\phi_{l_n} \hat{a}_{l_n}^\dagger |i\rangle_{n-1}$. Note that the physical freedom of the quantum emitter can be neglected temporally in this procedure since it can be added by expanding the physical dimension of the Sth site (see Appendix A 1 b).

The next step is to construct the matrix-product operator (MPO) for $e^{-i\hat{H}\tau}$, i.e.,

$$\hat{O}_\tau^{[n]} = \sum_{\{\sigma, \sigma'\}} Q_1^{[n]\sigma_1 \sigma_1'} Q_2^{[n]\sigma_2 \sigma_2'} \cdots Q_L^{[n]\sigma_L \sigma_L'}$$

$$\times |\sigma_1 \sigma_2 \cdots \sigma_L\rangle \langle \sigma_1' \sigma_2' \cdots \sigma_L'|, \tag{7}$$

where τ is a short time and $Q_l^{[n]\sigma_l \sigma_l'}$ is a matrix with $0 \leqslant \sigma_l, \sigma_l' \leqslant n$. Its tensor network is denoted in Fig. 1(c). The second-order Trotter decomposition is used, that is, $e^{-i\hat{H}\tau} \approx e^{-i\hat{H}_{\text{odd}}\tau/2} e^{-i\hat{H}_{\text{even}}\tau} e^{-i\hat{H}_{\text{odd}}\tau/2}$ [40], where $\hat{H}_{\text{odd}}$ and $\hat{H}_{\text{even}}$ are the Hamiltonians of the odd and even bonds, respectively.

For convenience, the Hamiltonian of the lth bond is denoted as $\hat{h}_l$. Since $[\hat{h}_l, \hat{h}_{l+2}] = 0$, the equations $e^{-i\hat{H}_{\text{odd}}\tau/2} \equiv e^{-i\hat{h}_1\tau/2} e^{-i\hat{h}_3\tau/2} \cdots$ and $e^{-i\hat{H}_{\text{even}}\tau} \equiv e^{-i\hat{h}_2\tau} e^{-i\hat{h}_4\tau} \cdots$ are strict; their last terms are determined by the parity of L. The method for constructing the MPO of $e^{-i\hat{h}_l\tau}$ is shown in Appendix A 2.

The time evolution of the MPS can be implemented by iteratively applying the MPO of $e^{-i\hat{H}\tau}$ on $|i\rangle_n$ (see Appendix A 3). The calculation errors primarily stem from Trotter decomposition and the truncation of both the MPS and MPO [42,47,55]. They can be mitigated by decreasing the time step and increasing the matrix dimensions of the MPS and MPO; see the convergence test of the calculation in Appendix A 4. For all the calculated results in this work, the deviations of the total occupation numbers from their initial values always remain below 0.01.

III. RESULTS AND DISCUSSION

A. Time evolution of photon-number distribution

With the above MPS method, the system state at time t (units of $\tau_0 = d/J$) can be obtained by applying $\hat{O}_\tau^{[n]}$ on $|i\rangle_n$ a total of t/τ times. Accordingly, the photon-number distributions $n_l \equiv \langle \hat{a}_l^\dagger \hat{a}_l \rangle$ can be found; see the cases for $n = 2$ and 10 in Fig. 2, where ε_0 is tuned with the quantum emitters, i.e., $\varepsilon_0 = \omega_c = \omega_a$. Figures 2(a) and 2(b) indicate that the transmission for the OC case is independent of n. However, unlike the OC, the TLA leads to a dependence of the transmission on n [see Figs. 2(c) and 2(d)]; that is, the transmission increases as n increases. On the contrary, the transmission decreases as n increases for the JCE case [see Figs. 2(e) and 2(f)]. That is because the JCE acts like an OC when n is much larger than 1. What is more, this method is universal and can be used for other types of incident pulses; see the double-peak pulses with $n = 2$ and 10 in Appendix B.

B. Transmission and correlation function

To explore the bunching and antibunching effects of the scattered states, we can calculate the second-order correlation function, i.e., $g_l^{(2)} \equiv \frac{\langle \hat{a}_l^\dagger \hat{a}_l^\dagger \hat{a}_l \hat{a}_l \rangle}{n_l^2}$ for the final state $|f\rangle_n$ after the scattering process. Note that $g_l^{(2)} \equiv 1 - \frac{1}{n}$ for any product Fock states $|i\rangle_n$ (see the proof in Appendix C). n_l/n and $g_l^{(2)}$ of $|f\rangle_n$ at $t = 160\tau_0$ are plotted in Fig. 3. For comparison, n_l/n of $|i\rangle_n$ is shown by the purple curve in Fig. 3(a). The MPS effectiveness is demonstrated by two known facts, namely, n_l/n in the OC-scattered states is independent of n [see the black curve in Fig. 3(a)], and the scattering of OCs does not change $g_l^{(2)}$ [see the two curves in Fig. 3(b)]. The latter fact implies that the OCs cannot break the straight-product property of the initial Fock states or induce photon-photon correlation.

However, the circumstances for TLAs and JCEs are changed [see Figs. 3(c)–3(f)]. The dependence of n_l/n and $g_l^{(2)}$ on n shows that the photon-photon correlation is induced. When $n = 1$, there is no photon-photon correlation, and thus, the distribution n_l/n in the TLA case is identical to that in the OC case [compare the black lines in Figs. 3(a) and 3(c)]. Because of the single-excitation property of TLAs, the transmission grows as n increases in Fig. 3(c). The stimulated and
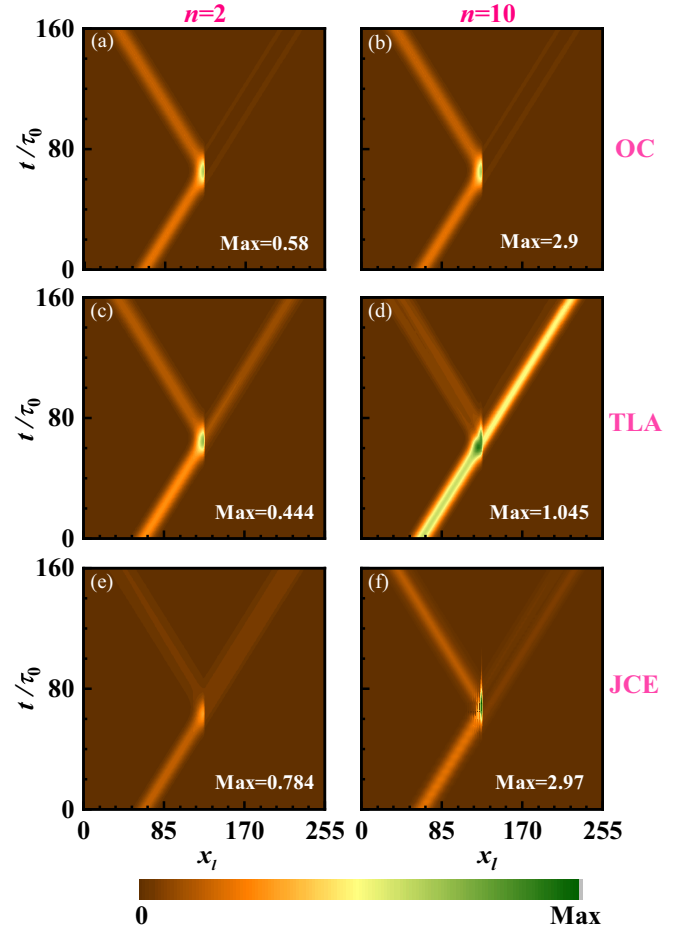

FIG. 2. Variations of the photon-number distributions with time scattered by (a) and (b) OCs, (c) and (d) TLAs, and (e) and (f) JCEs. The total photon number $n = 2$ ($n = 10$) for the left (right) column. Parameters: $L = 256$, $S = 128$, $k_0 = 0.5\pi$, $k_w = 0.05\pi/d$, $x_0 = 64d$, $\omega_a = \omega_c = \omega_W$, $V_0 = 0.4J$, and $\Omega = 0.15J$.

spontaneous emissions of TLAs are, respectively, responsible for the bunching of the transmitted photons ($g_l^{(2)} > 1$) and the antibunching of the reflected photons ($g_l^{(2)} < 1$) when $n = 2$ [see the blue line in Fig. 3(d)] [29]. As $n \to \infty$, the single-excitation property of the TLA results in most of the incident photons being transmitted without feeling the TLA. That is, $g_l^{(2)}$ should gradually approach 1 for the transmitted photons, becoming larger than 1 for the reflected ones [see the red line in Fig. 3(d)].

The transmission in the JCE case decreases as n increases, the opposite of what occurs in the TLA case [see Figs. 3(c) and 3(e)]. This is due to the JCEs being a composite of an OC and a TLA. Once the TLA is excited by a photon, the OC will dominate the scattering of the remaining photons. Accordingly, as $n \to \infty$, the distribution of n_l/n in the JCE case tends to that in the OC one [compare the red line in Fig. 3(e) with the black line in Fig. 3(a)]. JCEs also lead to different bunching and antibunching behaviors from those induced by TLAs. For example, the transmitted and reflected photons for $n = 2$ in Fig. 3(f) are antibunching ($g_l^{(2)} < 1$) and bunching ($g_l^{(2)} > 1$), respectively, the opposite of those in Fig. 3(d). Because the TLA no longer strongly influences
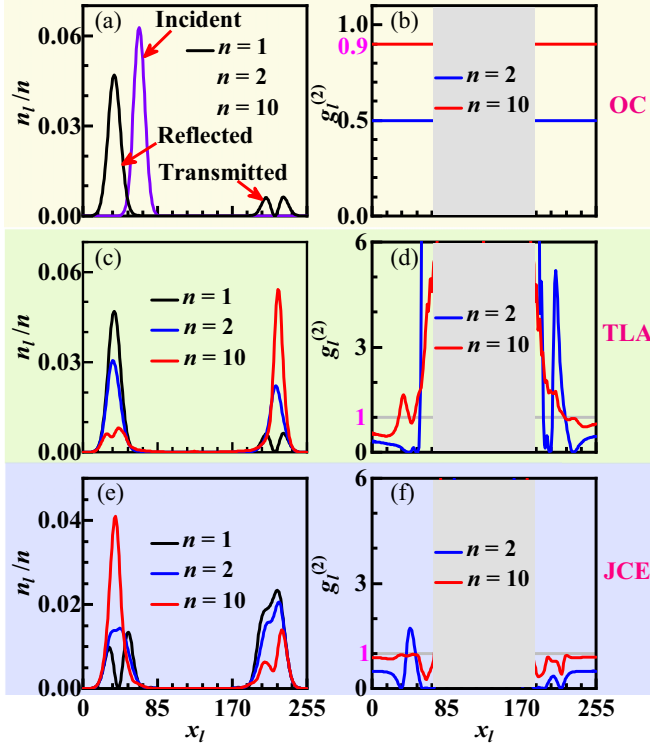
FIG. 3. Normalized photon-number distribution (left column) and second-order correlation functions (right column) of the final n-photon states scattered by (a) and (b) OCs, (c) and (d) TLAs, and (e) and (f) JCEs. The gray regions in the right column are not considered because all n_l are small in them. The parameters are identical to those in Fig. 2.

FIG. 4. (a) Variation of the transmission scattered by a JCE with n (black squares) with respect to that of $T_c + (T_J - T_c)/n$ (red circles). (b) Difference between the black squares and red circles in (a). The gray lines and dots in (a) and (b) show the limitation of $n \rightarrow \infty$. The parameters are identical to those in Fig. 2.

the incident states as $n \rightarrow \infty$, $g_l^{(2)}$ approaches unity for both transmitted and reflected photons [see the red line in Fig. 3(f)]. Accordingly, it is the OC rather than the TLA in the JCE that predominantly governs the scattering process when $n \rightarrow \infty$, fully different from few-photon cases. These physical behaviors remain the same for the incident pulse with double peaks (see Appendix B).

The above discussion yields two points that merit further exploration. First, given that OCs do not induce photon-photon correlation and the scattering effect of a JCE tends to that of an OC as $n \rightarrow \infty$, how does the photon-photon correlation strength induced by JCEs vary with n? Second, how do OCs, TLAs, and JCEs affect the phenomenon of photon bunching from the perspective of the occupation ratio of bunching photons?

C. Correlation effect of the JCE

This section explores the first point from the perspective of transmission, i.e., $T = \sum_{l>S} n_l/n$ for the final state, taking the tuning case of $\varepsilon_0 = \omega_c = \omega_a$ as an example. The transmission decreases as n increases [see the black line with squares in Fig. 4(a), whose horizontal axis is inversely proportional]. Such a transmission decrease should be attributed to the photon-photon correlation induced by the TLA in the JCE. As $n \gg 1$, the TLA in the JCE is consistently excited during the scattering process and no longer significantly impacts the
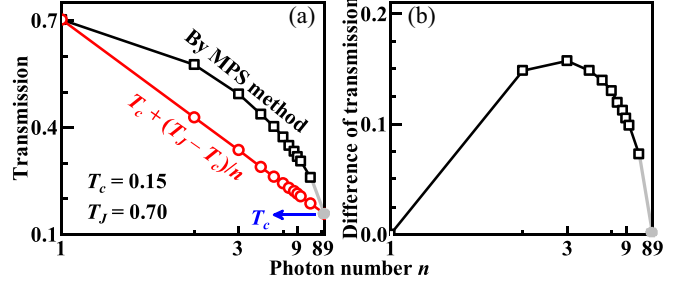
transmission, resulting in the transmission being primarily determined by the OC. If we neglect the photon-photon correlation, that is, assume that only the first arriving photon is scattered by the JCE while all the rest are scattered by the OC, we can deduce that the transmission of an n-photon pulse equals $[T_J + (n-1)T_c]/n = T_c + (T_J - T_c)/n$, where T_c and T_J are the transmissions of the single-photon state (i.e., $|i\rangle_1$) scattered by the OC and JCE, respectively. The expression of $T_c + (T_J - T_c)/n$ is plotted as the red line with circles in Fig. 4(a). Both lines converge toward T_c as $n \rightarrow \infty$ (see the gray dot). Since the photon-photon correlation is fully neglected in the red line with circles, the difference between the two lines in Fig. 4(a), illustrated in Fig. 4(b), reflects the strength of the photon-photon correlation induced by the JCE. The bump in the transmission difference implies that the photon-photon correlation exerts a strong influence on the incident pulse as it holds several particles.

D. Occupation ratio of bunching photons

This section focuses on how the three types of quantum emitters influence photon bunching behaviors, using the occupation ratio of bunching photons in n-photon states. The occupation ratio of $|\sigma_l\rangle_n$ is defined as $\rho_l^{[n]}(\sigma_l) = |_n\langle\sigma_l|f\rangle_n|^2$ (see Fig. 5 for $n = 2$ and 10). When $n = 2$ (the left column), the probability of $|2\rangle_2$ is always far less than that of $|1\rangle_2$ for all OC, TLA, and JCE cases, even as $g_l^{(2)} > 1$ [see Figs. 3(d) and 3(f)]. This is because the probability of $|0\rangle_2$ approaches 1, leading to $\rho_l^{[2]}(1) \ll 1$. Using $\rho_l^{[2]}(\sigma_l)$, we have

$$g_l^{(2)} = \frac{2\rho_l^{[2]}(2)}{\{\rho_l^{[2]}(1) + 2\rho_l^{[2]}(2)\}^2}.$$

Since both $\rho_l^{[2]}(1)$ and $\rho_l^{[2]}(2)$ are far less than 1, $g_l^{(2)} > 1$ as long as $\rho_l^{[2]}(2) \gtrsim 0.5\{\rho_l^{[2]}(1)\}^2$ and subsequently, $\rho_l^{[2]}(2) \ll \rho_l^{[2]}(1) \ll 1$. As n increases, the probabilities of $|\sigma_l \geqslant 2\rangle_n$ increase remarkably (comparing the left and right columns in Fig. 5).

The occupation ratio of bunching photons in multiphoton states, $\eta_l^{[n]} = 1 - \frac{1}{n_l}\rho_l^{[n]}(1)$, is plotted in the left column of Fig. 6. For three types of quantum emitters, we can roughly say that all $\eta_l^{[n]}$ increase as n increases. However, this variation behavior is not consistent with that of $g_l^{(2)}$ (compare
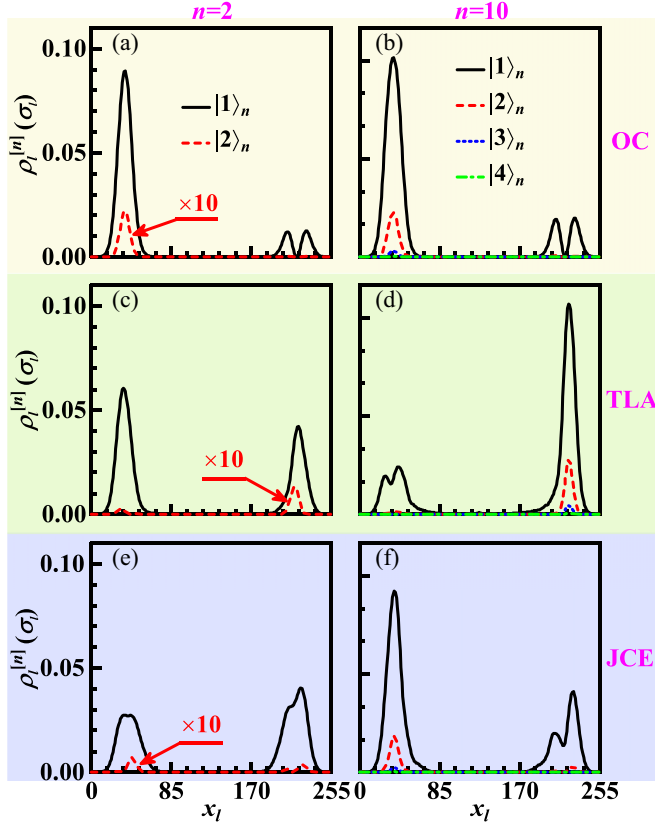
FIG. 5. Occupation probabilities of Fock states on every site in the final states $\rho_l^{[n]}(\sigma_l)$. The parameters are identical to those in Fig. 2.
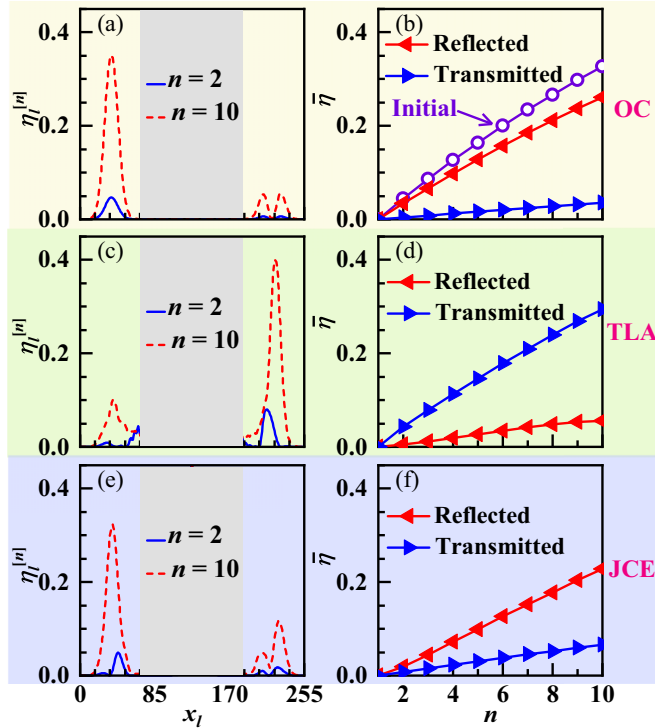

FIG. 6. $\eta_l^{[n]}$ (left column) and $\bar{\eta}$ (right column) of the final states scattered by (a) and (b) OCs, (c) and (d) TLAs, and (e) and (f) JCEs. The gray regions in left column are not considered because all n_l are small in them. The parameters are identical to those in Fig. 2.

the right column of Fig. 3 with the left column of Fig. 6). Such inconsistence implies that $g_l^{(2)}$ cannot fully capture the photon-bunching behavior. To measure the photon-bunching behaviors of the transmitted and reflected pulses, we therefore turn to the average occupation ratios of bunching photons, which are defined as $\bar{\eta}_t = \frac{\sum_{l>S} n_l \eta_l^{[n]}}{\sum_{l>S} n_l}$ and $\bar{\eta}_r = \frac{\sum_{l<S} n_l \eta_l^{[n]}}{\sum_{l<S} n_l}$ for the transmitted and reflected pulses, respectively.

In the right column of Fig. 6, $\bar{\eta}_t$ and $\bar{\eta}_r$ are plotted as a function of n. They both monotonously increase as n increases, and thus, the more photons the pulse includes, the greater the bunching behavior is. $g_l^{(2)}$ cannot lead to such a result (see the right column of Fig. 3). Some $g_l^{(2)}$ in the reflected pulse in the JCE case as $n = 2$ are evidently larger than those as $n = 10$ [see Fig. 3(f)]. In addition, $\bar{\eta}_t$ and $\bar{\eta}_r$ are always smaller than the average probabilities of bunching photons in the initial states [see Fig. 6(b)] for all three types of quantum emitters. Accordingly, the scattering process enhances the photon antibunching behavior from the perspective of multiphoton occupation. We also have $\bar{\eta}_r > \bar{\eta}_t$ for OCs and JCEs and $\bar{\eta}_r < \bar{\eta}_t$ for TLAs. These could be attributed to the transmitted and reflected pulses of the three cases having different photon-photon correlation and photon-bunching behavior.

IV. CONCLUSION AND OUTLOOK

MPS theory for the waveguide-QED systems was established to identify the statistics of tens-of-photons states scattered by OCs, TLAs, and JCEs. We showed that the scattering of OCs retains the straight-product property of the initial Fock states, i.e., $g_l^{(2)} \equiv 1 - \frac{1}{n}$, but changes the occupation ratio of bunching photons. However, both of them can be changed by the scattering of TLAs and JCEs, and therefore, TLAs and JCEs can induce photon-photon correlations, which leads to the variation of pulse forms, transmissions, and second-order correlation functions with n. Especially, we found that the scattering effects of JCEs tend to those of OCs when $n \to \infty$, and from the perspective of transmission there is a maximum in the photon-photon correlation induced by JCEs when the incident states involve several photons. What is more, different bunching and antibunching behaviors between few-photon and tens-of-photons cases were revealed. The occupation ratio of the bunching photons in the scattered states monotonously grows as the photon number increases for all three types of quantum emitters but is always less than that in the initial states.

Multiphoton interference [56,57] is a key resource in photonic quantum information processing [58,59], which plays a basic role in the task of multiphoton quantum key distributions [60], simulations [61], entanglement generations [18,25,57], and computations [57], among others [58,59]. This work developed the MPS method for quantum waveguides to study multiphoton statistics, holding potential for promoting the research of quantum informatics and techniques.

APPENDIX A: DETAILS OF THE CALCULATION

1. Constructing $|i\rangle_n$ in MPS form

The n-photon initial state considered is written in Eq. (6), whose Hilbert space grows exponentially as the photon number increases. In this section, we introduce the specific procedures for constructing the n-photon initial state $|i\rangle_n$ in the MPS form.

a. Direct construction

Let us consider a Fock state with n photons distributed among m sites. These sites are labeled i_1, i_2, $\ldots$, and i_m, with the corresponding occupation states denoted as $|n_{i_1}, n_{i_2}, \ldots, n_{i_m}\rangle$. The MPS representation of $|n_{i_1}, n_{i_2}, \ldots, n_{i_m}\rangle$ reads

$$|n_{i_1}, n_{i_2}, \ldots, n_{i_m}\rangle = \sum_{\{\sigma\}} M_1^{[n]\sigma_1} M_2^{[n]\sigma_2} \cdots M_L^{[n]\sigma_L} |\sigma_1 \sigma_2 \cdots \sigma_L\rangle, \tag{A1}$$

where the total photon number $n = \sum_{\alpha=1}^m n_{i_\alpha}$. The matrices have the form

$$M_l^{[n]\sigma_l} = \begin{cases} 1, & \sigma_l = n_l, \\ 0, & \sigma_l \neq n_l, \end{cases} \quad l \in \{i_1, i_2, \ldots, i_m\},$$
$$M_l^{[n]\sigma_l} = \begin{cases} 1, & \sigma_l = 0, \\ 0, & \sigma_l \neq 0, \end{cases} \quad l \notin \{i_1, i_2, \ldots, i_m\}. \tag{A2}$$

Using the above method, we are able to construct the MPS for arbitrary Fock states and thus their superposition. Let us take the superposition of $\mathcal{J}$ MPSs, denoted $|a_j\rangle$, as

$$|A\rangle = \sum_{j=1}^{\mathcal{J}} C_j |a_j\rangle, \tag{A3}$$

where the MPS for the Fock state $|a_j\rangle$ has the form

$$|a_j\rangle = \sum_{\{\sigma\}} M_{[j]1}^{[n]\sigma_1} M_{[j]2}^{[n]\sigma_2} \cdots M_{[j]L}^{[n]\sigma_L} |\sigma_1, \sigma_2, \ldots, \sigma_L\rangle. \tag{A4}$$

Here, the subscript $[j]$ denotes the jth Fock state. The MPS for the superposition state, denoted as

$$|A\rangle = \sum_{\{\sigma\}} A_1^{[n]\sigma_1} A_2^{[n]\sigma_2} \cdots A_L^{[n]\sigma_L} |\sigma_1, \sigma_2, \ldots, \sigma_L\rangle, \tag{A5}$$

can be obtained by the following transformation:

$$A_l^{[n]\sigma_l} = \begin{cases} \left(C_1^{\frac{1}{L}} M_{[1]l}^{[n]\sigma_l}, \ldots, C_{\mathcal{J}}^{\frac{1}{L}} M_{[\mathcal{J}]l}^{[n]\sigma_l}\right), & l = 1, \\ \left(C_1^{\frac{1}{L}} M_{[1]l}^{[n]\sigma_l}, \ldots, C_{\mathcal{J}}^{\frac{1}{L}} M_{[\mathcal{J}]l}^{[n]\sigma_l}\right)^T, & l = L, \\ \text{diag}\left(C_1^{\frac{1}{L}} M_{[1]l}^{[n]\sigma_l}, \ldots, C_{\mathcal{J}}^{\frac{1}{L}} M_{[\mathcal{J}]l}^{[n]\sigma_l}\right), & \text{else.} \end{cases} \tag{A6}$$

Hence, the MPS for

$$|i\rangle_n = \sum_{l_1, l_2, \ldots, l_n} \phi_{l_1} \phi_{l_2} \cdots \phi_{l_n} \hat{a}_{l_1}^\dagger \hat{a}_{l_2}^\dagger \cdots \hat{a}_{l_n}^\dagger |\varnothing\rangle$$

can be constructed in principle. However, the aforementioned approach is impractical in real operations due to the large number of Fock states involved in a superposition. For example, if there are three photons in the waveguide with $L = 256$, the number of Fock states is $C_L^1 + 2C_L^2 + C_L^3 = 2\,796\,416$. As a result, it is essential to find an efficient method for constructing the MPS (see the following section).

b. Iterative method

In the case of the Gaussian state given in Eq. (6), the iterative method relies on the relationship $|i\rangle_1 = \sum_{l_1} \phi_{l_1} \hat{a}_{l_1}^\dagger |\varnothing\rangle$. The detailed procedures are presented below.

Let us start by constructing the MPS for $|i\rangle_1$. First, we write the single-occupation state $\phi_{l_1} \hat{a}_{l_1}^\dagger |\varnothing\rangle$ in the MPS by taking its matrix set $\{M_{[l_1]l}^{[1]\sigma_l}\}$ as

$$M_{[l_1]l}^{[1]0} = \begin{cases} 1, & l \neq l_1, \\ 0, & l = l_1, \end{cases} \quad M_{[l_1]l}^{[1]1} = \begin{cases} 0, & l \neq l_1, \\ \phi_{l_1}, & l = l_1. \end{cases} \tag{A7}$$

For the superposition state $|i\rangle_1 = \sum_{l_1} \phi_{l_1} \hat{a}_{l_1}^\dagger |\varnothing\rangle$, the matrix set $\{M_l^{[1]\sigma_l}\}$ of the MPS representation can be written as

$$M_l^{[1]\sigma_l} = \begin{cases} \left(M_{[1]l}^{[1]\sigma_l}, M_{[2]l}^{[1]\sigma_l}, \cdots, M_{[L]l}^{[1]\sigma_l}\right), & l = 1, \\ \left(M_{[1]l}^{[1]\sigma_l}, M_{[2]l}^{[1]\sigma_l}, \cdots, M_{[L]l}^{[1]\sigma_l}\right)^T, & l = L, \\ \text{diag}\left(M_{[1]l}^{[1]\sigma_l}, M_{[2]l}^{[1]\sigma_l}, \cdots, M_{[L]l}^{[1]\sigma_l}\right), & \text{else.} \end{cases} \tag{A8}$$

That is,

$$|i\rangle_1 = \sum_{\{\sigma\}} M_1^{[1]\sigma_1} M_2^{[1]\sigma_2} \cdots M_L^{[1]\sigma_L} |\sigma_1, \sigma_2, \ldots, \sigma_L\rangle. \tag{A9}$$

Note that the superposition coefficients are involved in $\{M_{[l_1],l}^{[1]\sigma_l}\}$ [see Eq. (A7)].

The information provided thus far pertains to single-occupation states. For multioccupation states, one can derive the matrix set $\{M_{[l_n]l}^{[n]\sigma_l}\}$ for the state $\phi_{l_n} \hat{a}_{l_n}^\dagger |i\rangle_{n-1}$ from the matrix set $\{M_l^{[n-1]\sigma_l}\}$ associated with the state $|i\rangle_{n-1}$, using the relations

$$M_{[l_n]l}^{[n]\sigma_l} \xrightarrow{l=l_n} \begin{cases} \phi_{l_n} \sqrt{\sigma_l} M_l^{[n-1]\sigma_l-1}, & 1 \leqslant \sigma_l \leqslant n, \\ 0, & \sigma_l = 0, \end{cases} \tag{A10}$$

$$M_{[l_n]l}^{[n]\sigma_l} \xrightarrow{l \neq l_n} \begin{cases} 0, & \sigma_l = n, \\ M_l^{[n-1]\sigma_l}, & 0 \leqslant \sigma_l \leqslant n-1. \end{cases} \tag{A11}$$

Subsequently, the MPS representation for the superposition state involving $\phi_{l_n} \hat{a}_{l_n}^\dagger |i\rangle_{n-1}$ can be obtained through a procedure similar to Eq. (A8),

$$M_l^{[n]\sigma_l} = \begin{cases} \left(M_{[1]l}^{[n]\sigma_l}, M_{[2]l}^{[n]\sigma_l}, \ldots, M_{[L]l}^{[n]\sigma_l}\right), & l = 1, \\ \left(M_{[1]l}^{[n]\sigma_l}, M_{[2]l}^{[n]\sigma_l}, \ldots, M_{[L]l}^{[n]\sigma_l}\right)^T, & l = L, \\ \text{diag}\left(M_{[1]l}^{[n]\sigma_l}, M_{[2]l}^{[n]\sigma_l}, \ldots, M_{[L]l}^{[n]\sigma_l}\right), & \text{else.} \end{cases} \tag{A12}$$

Given the MPS representation of the single-occupation state $|i\rangle_1$ in Eq. (A9), one can derive the n-photon state $|i\rangle_n$ step by step.

The above iterative method does not include the quantum emitter. Here, we discuss how to incorporate the physical dimension of the quantum emitter. For site S, we treat the Sth cavity and the quantum emitter as a unified system. Consequently, the state space expands from σ_S to (σ_S, σ_c), (σ_S, σ_a), or $(\sigma_S, \sigma_c, \sigma_a)$ when considering an OC, a TLA, or a JCE, respectively. Here, σ_S represents the photon occupation number in the Sth cavity of the chain, σ_c denotes the photon occupation number in the OC, and σ_a indicates whether the TLA is excited or not. For the OC, when $\sigma_c = 0$, we have $M_S^{[n](\sigma_S, \sigma_c)} = M_S^{[n]\sigma_S}$; otherwise, $M_S^{[n](\sigma_S, \sigma_c)} = 0$. For the

TLA, when $\sigma_a = 0$, we have $M_S^{[n](\sigma_S,\sigma_a)} = M_S^{[n]\sigma_S}$; otherwise, $M_S^{[n](\sigma_S,\sigma_a)} = 0$. What is more, for the JCE, when $\sigma_c = \sigma_a = 0$, we have $M_S^{[n](\sigma_S,\sigma_c,\sigma_a)} = M_S^{[n]\sigma_S}$; otherwise, $M_S^{[n](\sigma_S,\sigma_c,\sigma_a)} = 0$. This approach can give the MPS representation for the n-photon initial state $|i\rangle_n$, as illustrated in Fig. 1(a).

It is crucial to note that the dimensions of the matrices will grow exponentially as we perform the procedure $|i\rangle_{n-1} \rightarrow |i\rangle_n$. Therefore, it becomes necessary to compress the matrices, typically achieved through singular-value decomposition (SVD), at each step. Moreover, for computational efficiency, it is highly advantageous to transform the MPS into either the left-canonical or right-canonical form during the process [42]. This canonicalization simplifies various calculations and reduces the computational cost associated with MPS-based methods.

2. Constructing $e^{-i\hat{H}\tau}$ in MPO form

In this section, we will outline the process of constructing the MPO for $e^{-i\hat{H}\tau}$ as given in Eq. (7).

We begin with the second-order Trotter decomposition,

$$e^{-i\hat{H}\tau} = e^{-i\hat{H}_{\text{odd}}\tau/2} e^{-i\hat{H}_{\text{even}}\tau} e^{-i\hat{H}_{\text{odd}}\tau/2} + O(\tau^3), \qquad (A13)$$

where $\hat{H}_{\text{odd}}$ and $\hat{H}_{\text{even}}$ represent the Hamiltonians acting on the odd and even bonds. They are

$$\hat{H}_{\text{odd}} = \sum_{l \in \text{odd}} \hat{h}_l, \quad \hat{H}_{\text{even}} = \sum_{l \in \text{even}} \hat{h}_l, \qquad (A14)$$

with

$$\hat{h}_l = \frac{1}{2}\omega_W(\hat{a}_l^\dagger \hat{a}_l + \hat{a}_{l+1}^\dagger \hat{a}_{l+1}) - \frac{J}{2}(\hat{a}_l^\dagger \hat{a}_{l+1} + \text{H.c.})$$
$$+ \begin{cases} \frac{1}{2}\omega_W(\hat{a}_1^\dagger \hat{a}_1 \delta_{l,1} + \hat{a}_L^\dagger \hat{a}_L \delta_{l,L-1}), & l \neq S-1, S, \\ \frac{1}{2}(\hat{H}_E + \hat{H}_I), & l = S-1, S. \end{cases} \qquad (A15)$$

Because $[\hat{h}_l, \hat{h}_{l+2}] = 0$, the equations $e^{-i\hat{H}_{\text{odd}}\tau/2} = e^{-i\hat{h}_1\tau/2} e^{-i\hat{h}_3\tau/2} \cdots$ and $e^{-i\hat{H}_{\text{even}}\tau} = e^{-i\hat{h}_2\tau} e^{-i\hat{h}_4\tau} \cdots$ are strict, and their last terms depend on the parity of L. After substituting the bond Hamiltonian $\hat{h}_l$ into $\hat{H}_{\text{odd}}$ and $\hat{H}_{\text{even}}$, our objective is to find the MPO for the operator of $e^{-i\hat{h}_l\tau}$, which can be solved using the following steps. First, calculate the matrix representation of $e^{-i\hat{h}_l\tau}$ on the basis set of $\{|\sigma_l, \sigma_{l+1}\rangle\}$, denoted as $D_{(\sigma_l \sigma_{l+1}),(\sigma_l' \sigma_{l+1}')}^{[n]} = \langle \sigma_l, \sigma_{l+1}|e^{-i\hat{h}_l\tau}|\sigma_l', \sigma_{l+1}'\rangle$, where σ_l is the physical index of the lth site. Then, exchange its second and third subscripts to get $\bar{D}_{(\sigma_l \sigma_l'),(\sigma_{l+1}\sigma_{l+1}')}^{[n]}$. Third, decompose $\bar{D}_{(\sigma_l \sigma_l'),(\sigma_{l+1}\sigma_{l+1}')}^{[n]}$ into the form

$$\bar{D}_{(\sigma_l \sigma_l'),(\sigma_{l+1}\sigma_{l+1}')}^{[n]} = \sum_{d_s=1}^{D_s} U_{(\sigma_l \sigma_l'),d_s}^{[n]} V_{d_s,(\sigma_{l+1}\sigma_{l+1}')}^{[n]\dagger} \qquad (A16)$$

using the SVD, where D_s is the number of the nonzero singular values. Note that the singular values have been moved into U and/or V. Finally, the matrices of the MPO on the lth and $(l+1)$th sites can be obtained by reshaping $U^{[n]}$ and $V^{[n]\dagger}$, that is,

$$U^{[n]} \rightarrow \left(Q_l^{[n]\sigma_l \sigma_l'}\right)_{1,D_s}, \quad V^{[n]\dagger} \rightarrow \left(Q_{l+1}^{[n]\sigma_{l+1}\sigma_{l+1}'}\right)_{D_s,1}.$$

Accordingly, the MPO for $e^{-i\hat{h}_l\tau}$ can be expressed as

$$e^{-i\hat{h}_l\tau} = \sum_{\{\sigma_l \sigma_{l+1}\}} \sum_{\{\sigma_l' \sigma_{l+1}'\}} Q_l^{[n]\sigma_l \sigma_l'} Q_{l+1}^{[n]\sigma_{l+1}\sigma_{l+1}'}$$
$$\times |\sigma_l, \sigma_{l+1}\rangle\langle\sigma_l', \sigma_{l+1}'|. \qquad (A17)$$

The procedure is similar for $e^{-i\hat{h}_l\tau/2}$. Using Eq. (A17), the MPO for both $e^{-i\hat{H}_{\text{odd}}\tau/2}$ and $e^{-i\hat{H}_{\text{even}}\tau}$ can be obtained, that is,

$$e^{-i\hat{H}_{\text{odd}}\tau/2} = \sum_{\{\sigma,\sigma'\}} Q_{\text{odd},1}^{[n]\sigma_1\sigma_1'} Q_{\text{odd},2}^{[n]\sigma_2\sigma_2'} \cdots Q_{\text{odd},L}^{[n]\sigma_L\sigma_L'}$$
$$\times |\sigma_1\sigma_2\cdots\sigma_L\rangle\langle\sigma_1'\sigma_2'\cdots\sigma_L'|, \qquad (A18)$$

$$e^{-i\hat{H}_{\text{even}}\tau} = \sum_{\{\sigma,\sigma'\}} Q_{\text{even},1}^{[n]\sigma_1\sigma_1'} Q_{\text{even},2}^{[n]\sigma_2\sigma_2'} \cdots Q_{\text{even},L}^{[n]\sigma_L\sigma_L'}$$
$$\times |\sigma_1\sigma_2\cdots\sigma_L\rangle\langle\sigma_1'\sigma_2'\cdots\sigma_L'|. \qquad (A19)$$

Then the matrices of the MPO in Eq. (A13) have the form

$$Q_l^{[n]\sigma_l\sigma_l'''} = \sum_{\sigma_l'\sigma_l''} Q_{\text{odd},l}^{[n]\sigma_l\sigma_l'} \otimes Q_{\text{even},l}^{[n]\sigma_l'\sigma_l''} \otimes Q_{\text{odd},l}^{[n]\sigma_l''\sigma_l'''}, \qquad (A20)$$

where $\otimes$ represents the Kronecker product between matrices.

In this way, the MPO of $e^{-i\hat{H}\tau}$ is successfully constructed, namely,

$$e^{-i\hat{H}\tau} = \sum_{\{\sigma,\sigma'\}} Q_1^{[n]\sigma_1\sigma_1'} Q_2^{[n]\sigma_2\sigma_2'} \cdots Q_L^{[n]\sigma_L\sigma_L'}$$
$$\times |\sigma_1\sigma_2\cdots\sigma_L\rangle\langle\sigma_1'\sigma_2'\cdots\sigma_L'|. \qquad (A21)$$

3. Time evolution

Once the n-photon initial MPS $|i\rangle_n$ and time evolution MPO $e^{-i\hat{H}\tau}$ are constructed, the MPS of $|\Phi(t+\tau)\rangle$ at time $t+\tau$ can be obtained by applying the MPO to the MPS of $|\Phi(t)\rangle$ at time t. The method of direct application [42] is used in this work, i.e.,

$$\hat{O}_\tau^{[n]}|\Phi(t)\rangle_n = \sum_{\{\sigma,\sigma'\}} \sum_{\{\alpha\}} Q_{1;\alpha_0,\alpha_1}^{[n]\sigma_1\sigma_1'} Q_{2;\alpha_1,\alpha_2}^{[n]\sigma_2\sigma_2'} \cdots Q_{L;\alpha_{L-1},\alpha_L}^{[n]\sigma_L\sigma_L'}$$
$$\times |\sigma_1, \sigma_2, \ldots, \sigma_L\rangle\langle\sigma_1', \sigma_2', \cdots, \sigma_L'|$$
$$\times \sum_{\{\sigma''\}} \sum_{\{\beta\}} M_{1;\beta_0,\beta_1}^{[n],\sigma_1''} M_{2;\beta_1,\beta_2}^{[n],\sigma_2''} \cdots M_{L;\beta_{L-1},\beta_L}^{[n],\sigma_L''}$$
$$\times |\sigma_1'', \sigma_2'', \ldots, \sigma_L''\rangle$$
$$= \sum_{\{\sigma\}} \sum_{\{\alpha,\beta\}} M_{1;\alpha_0\beta_0,\alpha_1\beta_1}^{'[n]\sigma_1} M_{2;\alpha_1\beta_1,\alpha_2\beta_2}^{'[n]\sigma_2} \cdots$$
$$\times M_{L;\alpha_{L-1}\beta_{L-1},\alpha_L\beta_L}^{'[n]\sigma_L} |\sigma_1, \sigma_2, \ldots, \sigma_L\rangle$$
$$= \sum_{\{\sigma\}} \sum_{\{\gamma\}} M_{1;\gamma_0,\gamma_1}^{'[n]\sigma_1} M_{2;\gamma_1,\gamma_2}^{'[n]\sigma_2} \cdots M_{L;\gamma_{L-1},\gamma_L}^{'[n]\sigma_L}$$
$$\times |\sigma_1, \sigma_2, \ldots, \sigma_L\rangle$$
$$\equiv |\Phi(t+\tau)\rangle_n. \qquad (A22)$$

The matrix $M_l^{'[n]\sigma_l}$ is given by

$$M_{l;\gamma_{l-1},\gamma_l}^{'[n]\sigma_l} = \sum_{\sigma_l'} Q_{l;\alpha_{l-1},\alpha_l}^{[n]\sigma_l\sigma_l'} M_{l;\beta_{l-1},\beta_l}^{[n],\sigma_l'}, \qquad (A23)$$
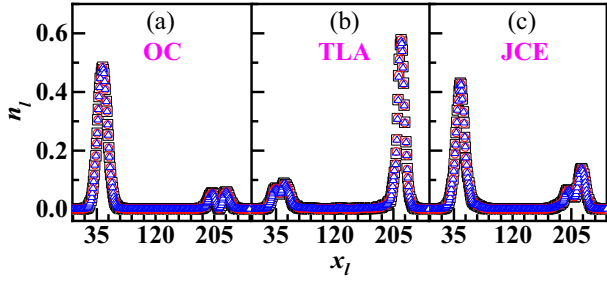
FIG. 7. Convergence of n_l for the final states scattered by (a) OCs, (b) TLAs, and (c) JCEs, respectively. The bond dimensions D are taken to be 25 (black squares), 27 (red circles), and 30 (blue triangles) in the calculations. The parameters are identical to those in Fig. 2.

where $\gamma_l = (\alpha_l \beta_l)$. The bond dimension of the matrices in the MPS increases every time the MPO is applied to it. The SVD is used to perform bond-dimension compression.

4. Convergence of the MPS method

In the whole process of calculating the final states $|f\rangle_n$, the computation complexity can be roughly measured by the element number of the MPS, i.e., $(n+1)[2D + (L-3)D^2] + Z_E$, with D being the bond dimension of the matrices. Here, $Z_E = (n+1)^2D^2$, $2(n+1)D^2$, and $2(n+1)^2D^2$ for the OC, TLA, and JCE cases, respectively. The choice of the value D is relevant to n. Generally, the larger n is, the larger D should be. In this section, we test the convergence of the MPS method

by calculating $n_l = {}_n\langle f|\hat{a}_l^\dagger \hat{a}_l|f\rangle_n$ for the final states scattered by the OC, TLA, and JCE (see Fig. 7).

The errors of the MPS method are mainly from Trotter decomposition and the truncations of the MPS and MPO. Figure 7 shows that the results of n_l are convergent as D reaches 25 for $n = 10$.

APPENDIX B: INCIDENT PULSE WITH DOUBLE PEAKS

To prove the universality of this method for other pulse types, we calculate n_l and $g_l^{(2)}$ for the incident pulses with double peaks, where $n = 2$ and 10 are taken as examples. The wave function of the incident pulse is $\phi_l' = N' \sum_k e^{-(k-k_0)^2/k_w^2} \{e^{-ik[x_l-(x_0+\Delta x)]} + e^{-ik[x_l-(x_0-\Delta x)]}\}$, with N' being the normalized constant and Δx being the center position shift. The results are shown in Fig. 8, presenting correlation behaviors similar to those of Gaussian pulses (see the right columns of Figs. 3 and 8).

Additionally, the MPS method developed here can also deal with other cases in the field of quantum waveguides, for example, a waveguide coupled to more than one quantum emitter. Another case is to analyze the decay of quantum waveguide systems. The decay effect can be introduced by two ways. One is to add an imaginary part to the eigenfrequency of each mode considered, such as $\tilde{\omega}_W = \omega_W - i\gamma_w/2$, with γ_w being the decay rate. The alternative approach involves employing the master equation, in which the MPS should be substituted with the MPO of the density matrix.
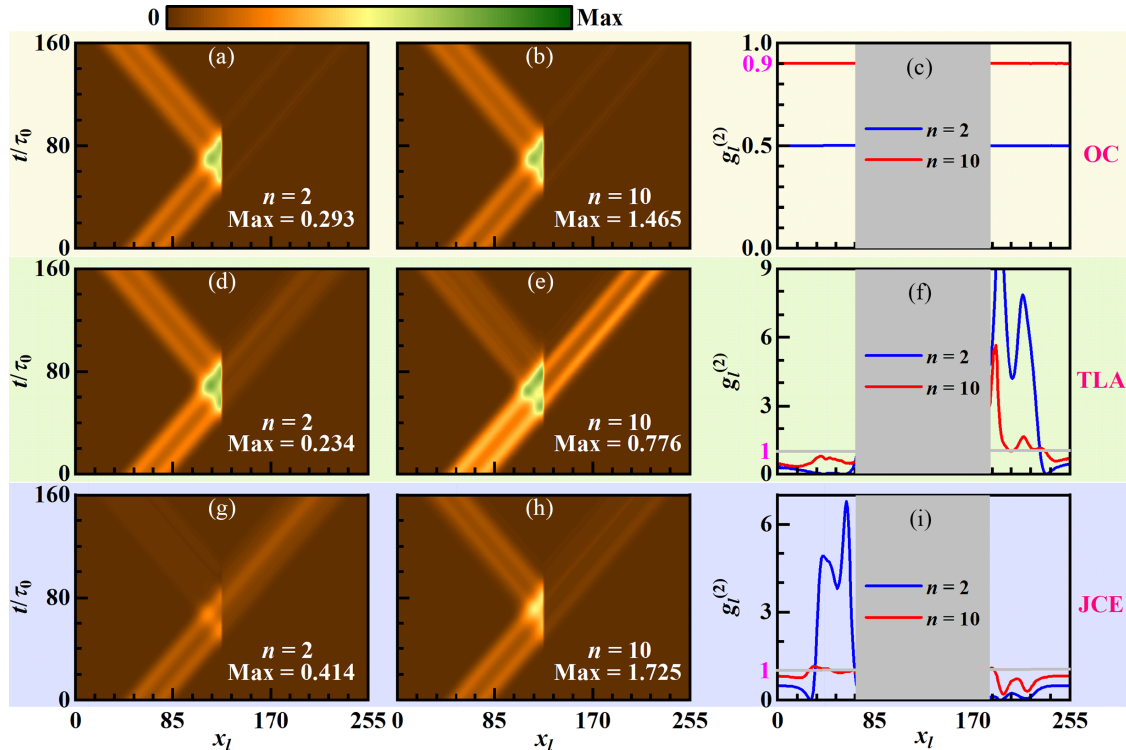

FIG. 8. Variations of n_l with time (left and middle columns) and $g_l^{(2)}$ at $t = 160\tau_0$ (right column) for (a)–(c) OCs, (d)–(f) TLAs, and (g)–(i) JCEs. The total photon number $n = 2$ ($n = 10$) for the left (middle) column and $\Delta x = 12$. The gray regions in the right column are not considered because all n_l are small in them. The parameters are identical to those in Fig. 2.
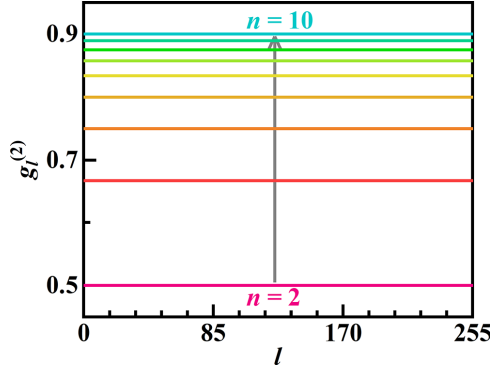
FIG. 9. Normalized second-order correlation functions for the n-photon product Fock state in Eq. (C1).

APPENDIX C: PROOF OF $g_l^{(2)} \equiv 1 - \frac{1}{n}$ FOR n-PHOTON PRODUCT FOCK STATES

In this Appendix, we investigate the second-order correlation function $g_l^{(2)}$ for an n-photon product Fock state, which does not have any photon-photon correlation between any photons. The state has a form similar to Eq. (6) in the main text, i.e.,

$$|\Psi\rangle_n = \sum_{l_1,l_2,...,l_n} \psi_{l_1}\psi_{l_2}\cdots\psi_{l_n}\hat{a}_{l_1}^\dagger\hat{a}_{l_2}^\dagger\cdots\hat{a}_{l_n}^\dagger|\varnothing\rangle, \quad (C1)$$

where ψ_l is a random number satisfying $\sum_l |\psi_l|^2 = 1$, which guarantees universality and normalization. We first consider the case of $n = 1$; the probabilities with one and zero photons on the lth site are taken to be $\rho_l^{[1]}(1)$ and $\rho_l^{[1]}(0) = 1 - \rho_l^{[1]}(1)$, respectively. For the n-photon case without photon-photon correlation, the probability of σ_l photons occupying the lth site can be written as

$$\rho_l^{[n]}(\sigma_l) = C_n^{\sigma_l}\{\rho_l^{[1]}(0)\}^{n-\sigma_l}\{\rho_l^{[1]}(1)\}^{\sigma_l}. \quad (C2)$$

Then $\langle\hat{n}_l\rangle$ and $\langle\hat{n}_l^2\rangle$ can be represented as

$$\langle\hat{n}_l\rangle = \sum_{\sigma_l=0}^n \sigma_l \rho_l^{[n]}(\sigma_l)$$

$$= \sum_{\sigma_l=0}^n \sigma_l C_n^{\sigma_l}\{\rho_l^{[1]}(0)\}^{n-\sigma_l}\{\rho_l^{[1]}(1)\}^{\sigma_l}, \quad (C3)$$

$$\langle\hat{n}_l^2\rangle = \sum_{\sigma_l=0}^n \sigma_l^2 \rho_l^{[n]}(\sigma_l)$$

$$= \sum_{\sigma_l=0}^n \sigma_l^2 C_n^{\sigma_l}\{\rho_l^{[1]}(0)\}^{n-\sigma_l}\{\rho_l^{[1]}(1)\}^{\sigma_l}. \quad (C4)$$

Substituting Eqs. (C3) and (C4) and $\rho_l^{[1]}(0) = 1 - \rho_l^{[1]}(1)$ into $g_l^{(2)} = \frac{\langle\hat{n}_l^2\rangle - \langle\hat{n}_l\rangle}{\langle\hat{n}_l\rangle^2}$ leads to $g_l^{(2)} \equiv 1 - \frac{1}{n}$. To confirm this, $g_l^{(2)}$ is plotted for the product Fock states in (C1) in Fig. 9, where ψ_l takes arbitrary value.

[1] G. Vidal, Efficient simulation of one-dimensional quantum many-body systems, Phys. Rev. Lett. **93**, 040502 (2004).

[2] J. Eisert, M. Friesdorf, and C. Gogolin, Quantum many-body systems out of equilibrium, Nat. Phys. **11**, 124 (2015).

[3] G. Carleo and M. Troyer, Solving the quantum many-body problem with artificial neural networks, Science **355**, 602 (2017).

[4] H. Weimer, A. Kshetrimayum, and R. Orús, Simulation methods for open quantum many-body systems, Rev. Mod. Phys. **93**, 015008 (2021).

[5] T. Felser, S. Notarnicola, and S. Montangero, Efficient tensor network ansatz for high-dimensional quantum many-body problems, Phys. Rev. Lett. **126**, 170603 (2021).

[6] D. Bluvstein, A. Omran, H. Levine, A. Keesling, G. Semeghini, S. Ebadi, T. T. Wang, A. A. Michailidis, N. Maskara, W. W. Ho, S. Choi, M. Serbyn, M. Greiner, V. Vuletić, and M. D. Lukin, Controlling quantum many-body dynamics in driven Rydberg atom arrays, Science **371**, 1355 (2021).

[7] J.-T. Shen and S. Fan, Strongly correlated two-photon transport in a one-dimensional waveguide coupled to a two-level system, Phys. Rev. Lett. **98**, 153003 (2007).

[8] V. I. Yudson and P. Reineker, Multiphoton scattering in a one-dimensional waveguide with resonant atoms, Phys. Rev. A **78**, 052713 (2008).

[9] J.-W. Pan, Z.-B. Chen, C.-Y. Lu, H. Weinfurter, A. Zeilinger, and M. Żukowski, Multiphoton entanglement and interferometry, Rev. Mod. Phys. **84**, 777 (2012).

[10] B. Q. Baragiola, R. L. Cook, A. M. Brańczyk, and J. Combes, n-photon wave packets interacting with an arbitrary quantum system, Phys. Rev. A **86**, 013811 (2012).

[11] T. Shi, D. E. Chang, and J. I. Cirac, Multiphoton-scattering theory and generalized master equations, Phys. Rev. A **92**, 053834 (2015).

[12] Ş. E. Kocabaş, Effects of modal dispersion on few-photon–qubit scattering in one-dimensional waveguides, Phys. Rev. A **93**, 033829 (2016).

[13] Z. Liao, Y. Lu, and M. S. Zubairy, Multiphoton pulses interacting with multiple emitters in a one-dimensional waveguide, Phys. Rev. A **102**, 053702 (2020).

[14] H.-S. Zhong et al., Quantum computational advantage using photons, Science **370**, 1460 (2020).

[15] J.-T. Shen and S. Fan, Theory of single-photon transport in a single-mode waveguide. I. Coupling to a cavity containing a two-level atom, Phys. Rev. A **79**, 023837 (2009).

[16] Z. Liao, X. Zeng, H. Nha, and M. S. Zubairy, Photon transport in a one-dimensional nanophotonic waveguide QED system, Phys. Scr. **91**, 063004 (2016).

[17] M. Bello, G. Platero, J. I. Cirac, and A. González-Tudela, Unconventional quantum optics in topological waveguide QED, Sci. Adv. **5**, eaaw0297 (2019).

[18] B. Kannan, D. L. Campbell, F. Vasconcelos, R. Winik, D. K. Kim, M. Kjaergaard, P. Krantz, A. Melville, B. M. Niedzielski, J. L. Yoder, T. P. Orlando, S. Gustavsson, and W. D. Oliver,

Generating spatially entangled itinerant photons with waveguide quantum electrodynamics, Sci. Adv. **6**, eabb8780 (2020).

[19] A. S. Sheremet, M. I. Petrov, I. V. Iorsh, A. V. Poshakinskiy, and A. N. Poddubny, Waveguide quantum electrodynamics: Collective radiance and photon-photon correlations, Rev. Mod. Phys. **95**, 015002 (2023).

[20] E. Waks and J. Vuckovic, Dipole induced transparency in drop-filter cavity-waveguide systems, Phys. Rev. Lett. **96**, 153601 (2006).

[21] T. Shi, S. Fan, and C. P. Sun, Two-photon transport in a waveguide coupled to a cavity in a two-level system, Phys. Rev. A **84**, 063803 (2011).

[22] H. Li, Z. Li, R. Zeng, M. Hu, M. Xu, X. Zhou, X. Xia, J. Xu, and Y. Yang, Single-photon switching in a Floquet waveguide-QED system with time-modulated coupling constants, Phys. Rev. A **107**, 023720 (2023).

[23] E. Rephaeli, Ş. E. Kocabaş, and S. Fan, Few-photon transport in a waveguide coupled to a pair of colocated two-level atoms, Phys. Rev. A **84**, 063832 (2011).

[24] Q. Hu, B. Zou, and Y. Zhang, Transmission and correlation of a two-photon pulse in a one-dimensional waveguide coupled with quantum emitters, Phys. Rev. A **97**, 033847 (2018).

[25] T. P. Rasmussen, Á. Rodríguez Echarri, J. D. Cox, and F. J. G. de Abajo, Generation of entangled waveguided photon pairs by free electrons, Sci. Adv. **10**, eadn6312 (2024).

[26] M. Hofheinz, E. M. Weig, M. Ansmann, R. C. Bialczak, and A. N. Cleland, Generation of Fock states in a superconducting quantum circuit, Nature (London) **454**, 310 (2008).

[27] J. C. Matthews, A. Politi, A. Stefanov, and J. L. O'brien, Manipulation of multiphoton entanglement in waveguide quantum circuits, Nat. Photon. **3**, 346 (2009).

[28] G. Park, I. Matsumoto, T. Kiyohara, H. F. Hofmann, R. Okamoto, and S. Takeuchi, Realization of photon correlations beyond the linear optics limit, Sci. Adv. **9**, eadj8146 (2023).

[29] Y. Shen and J.-T. Shen, Photonic-Fock-state scattering in a waveguide-QED system and their correlation functions, Phys. Rev. A **92**, 033803 (2015).

[30] I. M. Mirza and J. C. Schotland, Two-photon entanglement in multiqubit bidirectional-waveguide QED, Phys. Rev. A **94**, 012309 (2016).

[31] H. Zheng, D. J. Gauthier, and H. U. Baranger, Waveguide QED: Many-body bound-state effects in coherent and Fock-state scattering from a two-level system, Phys. Rev. A **82**, 063816 (2010).

[32] T. Shi and C. P. Sun, Lehmann-Symanzik-Zimmermann reduction approach to multiphoton scattering in coupled-resonator arrays, Phys. Rev. B **79**, 205111 (2009).

[33] T. Shi and S. Fan, Two-photon transport through a waveguide coupling to a whispering-gallery resonator containing an atom and photon-blockade effect, Phys. Rev. A **87**, 063818 (2013).

[34] T. F. See, C. Noh, and D. G. Angelakis, Diagrammatic approach to multiphoton scattering, Phys. Rev. A **95**, 053845 (2017).

[35] S. Fan, Ş. E. Kocabaş, and J.-T. Shen, Input-output formalism for few-photon transport in one-dimensional nanophotonic waveguides coupled to a qubit, Phys. Rev. A **82**, 063821 (2010).

[36] E. Rephaeli and S. Fan, Few-photon single-atom cavity QED with input-output formalism in Fock space, IEEE J. Sel. Top. Quantum Electron. **18**, 1754 (2012).

[37] S. Xu and S. Fan, Input-output formalism for few-photon transport: A systematic treatment beyond two photons, Phys. Rev. A **91**, 043845 (2015).

[38] K. B. Joanesarson, J. Iles-Smith, M. Heuck, and J. Mørk, Few-photon transport in Fano-resonance waveguide geometries, Phys. Rev. A **101**, 063809 (2020).

[39] P. W. Anderson, More is different: Broken symmetry and the nature of the hierarchical structure of science, Science **177**, 393 (1972).

[40] U. Schollwöck, The density-matrix renormalization group in the age of matrix product states, Ann. Phys. (NY) **326**, 96 (2011).

[41] R. Orús, A practical introduction to tensor networks: Matrix product states and projected entangled pair states, Ann. Phys. (NY) **349**, 117 (2014).

[42] S. Paeckel, T. Köhler, A. Swoboda, S. R. Manmana, U. Schollwöck, and C. Hubig, Time-evolution methods for matrix-product states, Ann. Phys. (NY) **411**, 167998 (2019).

[43] J. I. Cirac, D. Pérez-García, N. Schuch, and F. Verstraete, Matrix product states and projected entangled pair states: Concepts, symmetries, theorems, Rev. Mod. Phys. **93**, 045003 (2021).

[44] S. R. White, Density matrix formulation for quantum renormalization groups, Phys. Rev. Lett. **69**, 2863 (1992).

[45] S. R. White, Density-matrix algorithms for quantum renormalization groups, Phys. Rev. B **48**, 10345 (1993).

[46] T. H. Johnson, S. R. Clark, and D. Jaksch, Dynamical simulations of classical stochastic systems using matrix product states, Phys. Rev. E **82**, 036702 (2010).

[47] S. Singh, R. N. C. Pfeifer, G. Vidal, and G. K. Brennen, Matrix product states for anyonic systems and efficient simulation of dynamics, Phys. Rev. B **89**, 075112 (2014).

[48] P. P. Mazza, G. Perfetto, A. Lerose, M. Collura, and A. Gambassi, Suppression of transport in nondisordered quantum spin chains due to confined excitations, Phys. Rev. B **99**, 180302(R) (2019).

[49] A. J. Friedman, B. Ware, R. Vasseur, and A. C. Potter, Topological edge modes without symmetry in quasiperiodically driven spin chains, Phys. Rev. B **105**, 115117 (2022).

[50] M. Urbanek and P. Soldán, Parallel implementation of the time-evolving block decimation algorithm for the Bose-Hubbard model, Comput. Phys. Commun. **199**, 170 (2016).

[51] E. Sanchez-Burillo, D. Zueco, J. J. Garcia-Ripoll, and L. Martin-Moreno, Scattering in the ultrastrong regime: Nonlinear optics with one photon, Phys. Rev. Lett. **113**, 263604 (2014).

[52] E. Sánchez-Burillo, J. García-Ripoll, L. Martín-Moreno, and D. Zueco, Nonlinear quantum optics in the (ultra) strong light–matter coupling, Faraday Discuss. **178**, 335 (2015).

[53] E. Sánchez-Burillo, D. Zueco, L. Martín-Moreno, and J. J. García-Ripoll, Dynamical signatures of bound states in waveguide QED, Phys. Rev. A **96**, 023831 (2017).

[54] L. Qiao, Y.-J. Song, and C.-P. Sun, Quantum phase transition and interference trapping of populations in a coupled-resonator waveguide, Phys. Rev. A **100**, 013825 (2019).

[55] M. Suzuki, Generalized Trotter's formula and systematic approximants of exponential operators and inner derivations with applications to many-body problems, Commun. Math. Phys. **51**, 183 (1976).

[56] F. Flamini, M. Walschaers, N. Spagnolo, N. Wiebe, A. Buchleitner, and F. Sciarrino, Validating multi-photon quantum interference with finite data, Quantum Sci. Technol. **5**, 045005 (2020).

[57] X. Gu, L. Chen, and M. Krenn, Quantum experiments and hypergraphs: Multiphoton sources for quantum interference,

quantum computation, and quantum entanglement, Phys. Rev. A **101**, 033816 (2020).

[58] F. Flamini, N. Spagnolo, and F. Sciarrino, Photonic quantum information processing: A review, Rep. Prog. Phys. **82**, 016001 (2019).

[59] S. Slussarenko and G. J. Pryde, Photonic quantum information processing: A concise review, Appl. Phys. Rev. **6**, 041303 (2019).

[60] F. B. Basset, M. Valeri, E. Roccia, V. Muredda, D. Poderini, J. Neuwirth, N. Spagnolo, M. B. Rota, G. Carvacho, F. Sciarrino, and R. Trotta, Quantum key distribution with entangled photons generated on demand by a quantum dot, Sci. Adv. **7**, eabe6379 (2021).

[61] R. Puebla, J. Casanova, O. Houhou, E. Solano, and M. Paternostro, Quantum simulation of multiphoton and nonlinear dissipative spin-boson models, Phys. Rev. A **99**, 032303 (2019).